On the phase diagram of frustrated (quasi-)periodic cellular automata

1996 J. Phys. A: Math. Gen. 29 3021

(http://iopscience.iop.org/0305-4470/29/12/010)

J. Phys. A: Math. Gen. **29** (1996) 3021–3036. Printed in the UK

On the phase diagram of frustrated (quasi-)periodic cellular automata

Normand Mousseau†

Theoretical Physics, University of Oxford, 1 Keble Road, Oxford OX1 3NP, UK

Received 26 May 1995

Abstract. We introduce and study frustrated cellular automata (CA) obtained by quenching competing Chaté–Manneville rules. A period-two (P2) rule and a quasi-periodic one with period close to three (QP3) are frozen at random on the lattice sites. We find that the periodic and quasi-periodic cycles are resilient to internal frustration as well as to external unbounded noise. A low concentration of impurities improves the (quasi-)periodicity of the CA, damping the chaotic background noise significantly. Starting from pure QP3 CA, a first phase transition happens at a concentration of rule P2, $p(\text{P2}) \simeq 0.359$, leading to a macroscopic fixed point. A second phase transition, at $p(\text{P2}) \simeq 0.70$, brings the P2 phase. Although macroscopically stable, the central phase displays a stretched exponential relaxation of the site–site autocorrelations, indicating the presence of a new type of glass with slow dynamics superimposed on the natural cyclic dynamics of the CA rules. These results appear to be quite general and are found for many pairs of rules.

1. Introduction

Cellular automata (CA) have attracted attention over the last decade for a variety of reasons [1]: (i) since they are discrete objects in time, space and the number of states accessible, they can be studied exactly by numerical methods; (ii) in spite of their apparent simplicity, they remain a theoretical challenge and no general theory exists that can classify their macroscopic behaviour simply by looking at the local rules; (iii) the rules chosen are arbitrary so they offer a useful method for studying a wide range of non-equilibrium systems. With suitably selected evolution rules, CA can reproduce complex dynamical behaviour like avalanches or the Navier–Stokes equation [2]. Cellular automata therefore constitute a unique class of dynamical systems on which one can easily test concepts and methods of analysis.

For thermodynamical–equilibrium problems, Toulouse showed that frustration can play a fundamental role in the creation of complex phenomena [3] both in ordered and disordered problems. Since then, this concept has been very useful for a wide range of problems ranging from the ordered axial-next-nearest-neighbour Ising model (ANNNI) [4] to spin glasses [5]. Relatively little is known, however, about the effects of frustration or competition on dynamical systems. It is therefore interesting to see how much of the understanding gained in equilibrium physics can be transferred to dynamical systems.

In the present paper, extending previous results [6], we use simple periodic and quasi-periodic cellular automata to study the stability of time oscillating systems under introduction

† Present address: Département de physique and Groupe de recherche en physique et technologie des couches minces, Université de Montréal, CP 6128, Succ. Centre-ville, Montréal, Québec, Canada, H3C 3J7.

0305-4470/96/123021+16$19.50

of disturbances: external noise or internal frustration. Many complex non-equilibrium systems display a periodicity in time achieved via synchronization and collective behaviour. The interest of the specific CA studied here, first introduced by Chaté and Manneville [7, 8], is that although they display temporal periodicity macroscopically, they remain spatially homogeneous, allowing us to concentrate on one effect at a time.

We introduce frustration by quenching at random on the lattice two evolution rules leading to different time behaviours. We have selected a rule with periodicity two (P2) and a quasi-periodic one close to period three (QP3) which are attributed randomly to each site of the lattice and quenched there. For low concentration of the minority rule, the temporal behaviour remains controlled by the majority rule. When the two rules are present with roughly equal probability, a new phase appears which shows no macroscopic periodicity but displays stretched-exponential relaxation of the autocorrelation functions. These phases remain stable in the presence of a finite amount of external noise. Results presented here seem to be general in that they are found for many pairs of rules.

The structure of this paper is as follows. In the next section, we review the general properties of the Chaté and Manneville CA. In section 3, we examine the stability of the periodic and quasi-periodic phases under frustration in the deterministic limit. Section 4 presents, still at zero external noise, results for the glassy phase found at a large degree of frustration. In the following section, external unbounded noise is introduced and its effects discussed. Finally, in section 6 we show that many other rules present qualitatively similar effects.

2. The Chaté and Manneville CA

The cellular automata rules used in this paper were introduced by Chaté and Manneville a few years ago [7] and their properties studied extensively in a review article [8]. These models evolve following simple totalistic rules which are defined as

$$s_i(t+1) = \begin{cases} 1 & \text{if} \quad S_{\min} \leqslant \sum_{\mathcal{N}} s_j(t) \leqslant S_{\max} \\ 0 & \text{otherwise} \end{cases} \tag{1}$$

where $\mathcal{N}$ is the von Neumann neighbourhood (all the nearest neighbours plus the central site itself) on a cubic lattice and $S_{\min}$ and $S_{\max}$ specify the rule completely. For clarity, we use the notation introduced in [7] to identify a given rule $\mathcal{R}$,

$$\mathcal{R}^{d}_{S_{\min}-S_{\max}} \tag{2}$$

where d is the dimensionality of the lattice. All sites are updated in parallel. At $t = 0$, a (randomly chosen) fraction m_0 of the sites are set to 1, while the remaining sites are set to 0. Chaté and Manneville found that starting from such a disordered configuration it was possible to obtain complex cyclical behaviour with periodic and quasi-periodic oscillations of the magnetization, $m(t) = 1/N \sum_i s_i(t)$, where N is the number of sites on hypercubic lattices of dimension higher than three. The term *magnetization* is used by analogy with Ising spin models although here it is restricted to the interval $[0, 1]$. Models on hypercubic lattices of up to eight dimensions have been studied. Other totalistic rules leading to similar quasi-periodic behaviour in three dimensions have also been found [9]. Using an analogy between temporally periodic phases and the growth of smooth interfaces, Grinstein *et al* [10] have argued that quasi-periodic cycles should not exist in two or less dimensions, while periodic CA could exist only for specific rules where fluctuations are rendered unstable.

For more details about the behaviour of one-rule systems, we refer the reader to the excellent review by Chaté and Manneville [7]. Here we will just mention the most important

properties of these systems. (i) These CA can display non-trivial temporal behaviour when started from a random initial configuration. For a total magnetization between about a quarter and three quarters, the system will generally evolve into the same macroscopic state. (ii) In this macroscopic state, the total magnetization will either converge to a fixed point or to a limit cycle, periodic or quasi-periodic. (iii) The convergence is extremely quick: systems typically reach their limit cycle in only a few time steps, 10 or less. (iv) Microscopically, the lattice remains disordered and this disorder is reflected in the presence of some noise in the macroscopic parameter for finite N. This noise scales as $N^{1/2}$ [12] and therefore should vanish in the thermodynamical limit. (v) This specific type of rule leads to interesting behaviour only for high-dimensional lattices (four dimensions and higher).

One can write down a mean-field solution for the temporal evolution of the global magnetization [7],

$$m(t+1) = \sum_{r=S_{\min}}^{S_{\max}} \frac{N!}{r!(N-r)!} m(t)^r [1-m(t)]^{N-r} \tag{3}$$

which is simply an enumeration of the possible states of nearest neighbours for a random distribution of zeros and ones. This solution, plotted in figure 1, has only fixed points or chaotic solutions and does not reproduce the temporal behaviour of the real CA. As discussed in section 5, this equation describes the CA properly only at high external noise, when correlations vanish. We are still lacking a satisfying analytical solution for the time behaviour of these CA. Even allowing for multipoint correlation functions in their approximate theory, Chaté *et al* [11] find, for the Hemmingsson rule, a smooth, almost spherical, orbit instead of the characteristic triangular orbit obtained from the simulation, with a phase velocity differing from the exact simulation results.

In sections 3–5 of this paper we concentrate on a mixture of two specific rules: $\mathcal{R}^5_{5-8}$ and $\mathcal{R}^5_{1-9}$. $\mathcal{R}^5_{5-8}$ produces a quasi-periodic cycle in the magnetization with a period close to three and will be referred to as rule QP3 (figure 2(*a*)). $\mathcal{R}^5_{1-9}$ gives a period-two cycle which will be called P2 (figure 2(*b*)). As these two rules lead to incompatible time periodicity, we

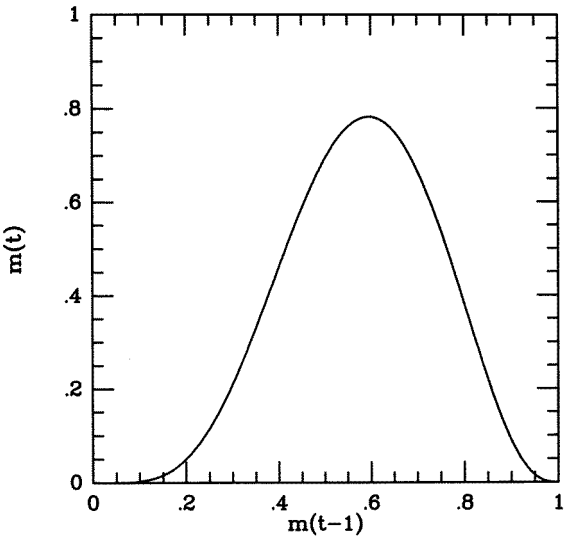

Figure 1. Magnetization map for the mean-field solution discussed in the text.

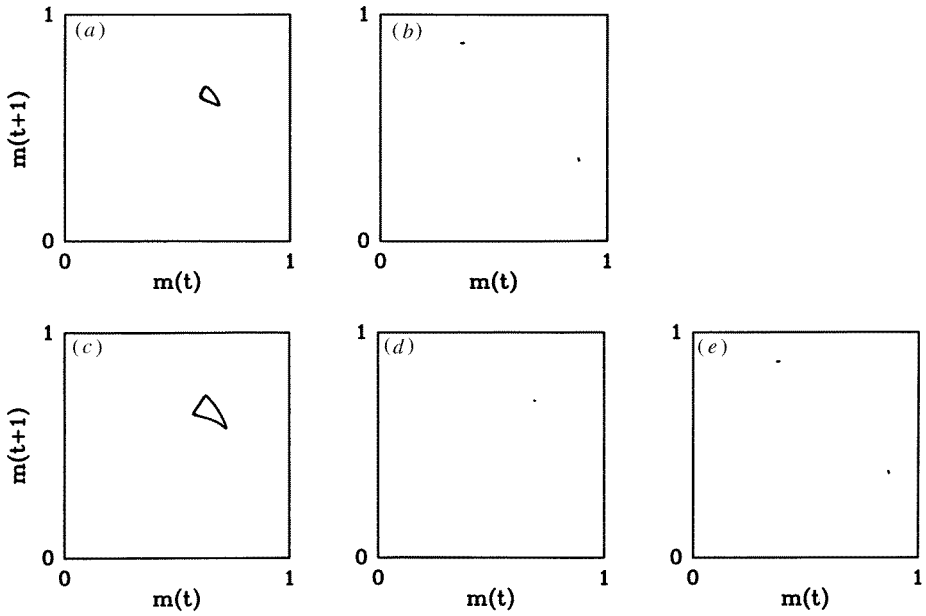

Figure 2. Magnetization map for a 20^5 site lattice at a concentration of rule P2: (*a*) $p = 0.00$, (*b*) 1.00, (*c*) 0.10, (*d*) 0.50 and (*e*) 0.90.

can introduce frustration in the CA by quenching them randomly on the lattice. Previous work has been done by Hemmingsson and Peng on a four-dimensional CA in which they mixed P3 and QP3 rules [13]. They found a second-order phase transition. In this work, the first comparable study of incompatible cycles, i.e. where one cannot go continuously from one cycle to the other, is presented. Other rules that have been surveyed will be discussed in the last section of this paper.

3. Effects of frustration at zero temperature

Here, we report the effect of mixing microscopic rules on the macroscopic order parameter $m(t)$. Before the start of the simulations, local rules are attributed to each site of the lattice: the P2 rule with probability p(P2) and the QP3 rule with probability $1 - p$(P2). Once assigned, the rules are quenched for the length of the simulation. A (randomly chosen) fraction $m(0) = 0.50$ of sites is then set to 1 for the initial configuration. The system is next evolved microscopically using parallel updating. The value of the initial magnetization is irrelevant as long as $m(0)$ is taken to be somewhere between about 0.25 and 0.75, with the precise bounds depending of the particular values of $S_{\min}$ and $S_{\max}$. Inside these bounds, the models always converge to the same attractor. The absorbing state, $m(t) = 0$, reached for an $m(0)$ which is either too low or too high, is unstable under the introduction of a large enough external noise. In the zero external noise limit, the dynamics is purely deterministic and randomness only enters in the distribution of the rules and in the choice of the initial value assigned to each site. As is the case for a one-rule (or pure) CA, the transient period of the frustrated CA is very short and the system rapidly evolves onto a stable orbit or a fixed point. The simulations were generally performed on lattices varying between $15^5 = 759\,375$ and $20^5 = 3\,200\,000$ sites, with a few simulations with $44^5 = 164$

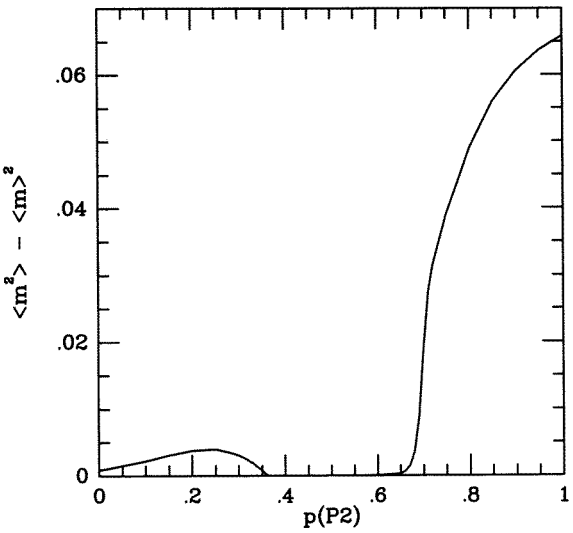

Figure 3. Variance of the magnetization as a function of the concentration of rule P2.

million sites for the autocorrelation functions. To be certain that the system was not in the transient phase, the first 500 time steps were discarded. This equilibration time is more than an order of magnitude larger than the usual transient time. As results are inherently noisy, it is simpler to discard more time steps than to identify accurately the moment when the magnetization falls onto the stable orbit. A highly efficient implementation was obtained by employing multispin coding. Writing the algorithm in bit operations that act on 32 sites in parallel, we reached a speed of about three iterations per second for a 20^5 site lattice on a Dec Alpha workstation.

As we vary the concentration of rule P2 (p(P2)), from pure QP3 to pure P2, in the absence of external noise, we find three different phases. At low p(P2), the quasi-periodic phase QP3 remains stable, with no sign of a period-two behaviour. As the concentration of rule P2 increases to the point where the two rules are distributed with roughly equal probability, the magnetization cycle collapses to a single dot. At high p(P2), a two-cycle appears, dominating the temporal behaviour.

We can follow the transition between these phases by looking at the size of the orbit in the magnetization map. For an infinitely large CA, for both periodic and quasi-periodic phases, this quantity should remain finite while it should be zero in a static phase. More precisely, the size of the orbit can be described by the fluctuations in the total magnetization

$$\Delta m = \langle m(t)^2 \rangle_t - \langle m(t) \rangle_t^2 . \tag{4}$$

Figure 3 shows the variations in this quantity as a function of p(P2).

Figure 2 displays the magnetization maps for five values of p(P2): 0, 0.10, 0.50, 0.90 and 1 belonging to the three phases described here. As is also found in the one-rule CA, an increase in size of the simulation cell leads to a decrease in the amplitude of the noise [12]. It is therefore expected that in the thermodynamic limit the dot in figure 2(d) will go to a point with no spatial extension. For the two other phases, the structure in the magnetization map should remain in the thermodynamical limit, but the width of the lines should go to zero.

Figure 4 displays the Fourier transform of the magnetization obtained in a sequence of

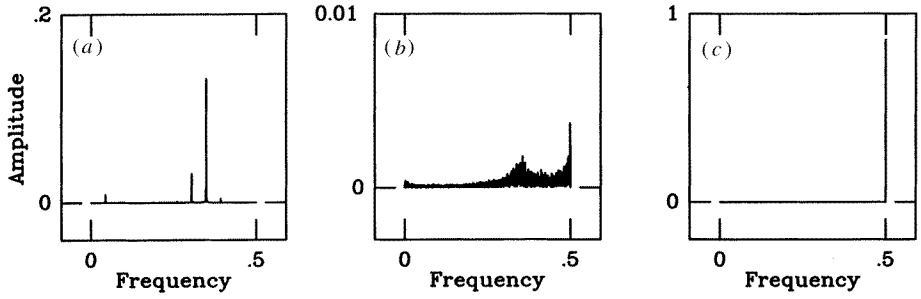

Figure 4. Frequency spectrum taken over 8192 time steps on a 20^5 site lattice for $p(\mathrm{P2})$: (*a*) 0.10, (*b*) 0.50 and (*c*) 0.90. Note the different scales.

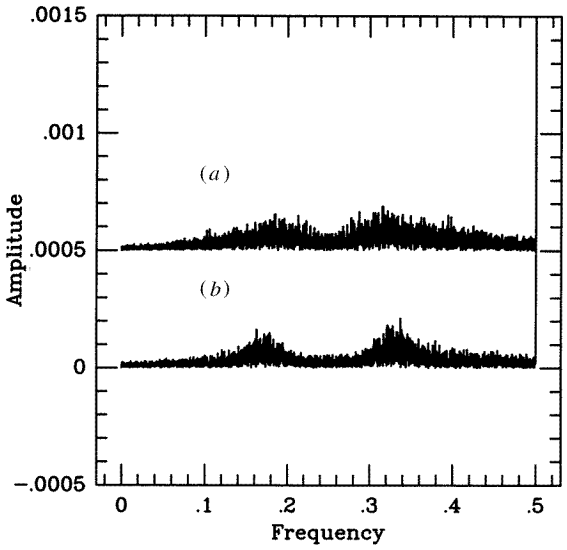

Figure 5. Blow up of the noisy tail of the frequency spectrum for (*a*) $p(\mathrm{P2}) = 1.00$ and (*b*) $p(\mathrm{P2}) = 0.90$. The scale has been shifted for more clarity.

8192 time steps for $p(\mathrm{P2}) = 0.10$, 0.50 and 0.90,

$$F = \sum \cos(kt)(m(t) - \langle m \rangle_t) \tag{5}$$

with the total amplitude normalized to 1. There is no trace of P2 at low concentration of this rule, nor is there any trace of QP3 for high $p(\mathrm{P2})$. In the middle section, the frequency spectrum is wide and the amplitude of the frequencies associated with the pure rules is comparable to the background, although there is a bias towards frequencies close to those found in the other two phases.

The effect of a small amount of impurities on the frequency spectrum is to decrease the amplitude of the noisy background against the dominant frequencies. For a pure $p(\mathrm{P2}) = 1$ CA, the amplitude of the peak at frequency $\frac{1}{2}$ is 0.837 while it is 0.863 when 10% of rule QP3 is introduced. As shown in figure 5, the weight in the dominant peak is gained at the expense of the internal noise which decreases noticeably when impurities are introduced. Similar results are found in the QP3 CA if small amounts of rule P2 are introduced. Therefore, impurities play a stabilizing role on the cycle, damping the macroscopic noise. Hakim and

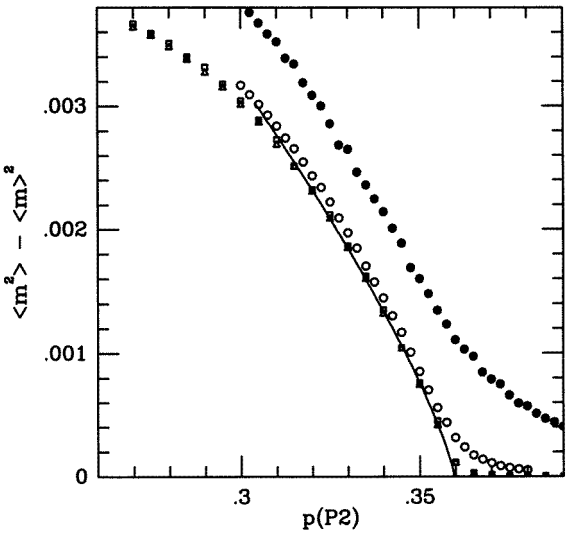

Figure 6. Variance of the magnetization as a function of the concentration of rule P2 around the QP3 to fixed-point transition for three system sizes: L^6 (full cicles), L^12 (open circles), L^16 (open squares) and L^24 (open triangles). The full curve is a fit to the scaling function with $p_c = 0.3595$ and $\gamma = 0.78$.

Rappel noticed recently [14] that the introduction of stochastic noise into globally coupled complex Ginzburg–Landau equations can induce periodic behaviour. For the present CA, the stabilizing factor comes from spatially quenched disorder rather than from external stochastic noise. This effect of impurities can also be found in the time domain; figure 3 shows that the insertion of sites following rules P2 on a predominantly QP3 lattice has the effect of increasing the size of the cycle by a factor of almost four.

We consider first the transition from QP3 to the fixed point phase. Figure 6 shows the variation of the order parameter for five lattices of different size. In each simulation, the run lasted 2500 time steps with the first 500 time steps rejected. For $L = 6$ and 12, results were averaged over 100 samples. Four samples were used for $L = 16$, 20 and 24. Lattices of $L = 16$ and larger display a very sharp transition point that is almost discontinuous. For smaller lattices, the macroscopic order parameter is dominated by noise. Making the scaling assumption for $p < p_c^{QP3}$,

$$\Delta m \sim (p_c^{QP3} - p)^{\gamma} \tag{6}$$

we find that to our degree of precision, p_c does not vary with L between $L = 16$ and $L = 24$. Its numerical value is $p_c^{QP3} = 0.3595 \pm 0.001$, with $\gamma = 0.78 \pm 0.05$ (table 1).

The second transition from the stable magnetization to the period-two cycle is first-order and consequently displays hysteresis (figure 7). To obtain this curve, we started with an $L = 16$ lattice at $p(P2) = 0.86$. After rejecting the first 250 time steps, we calculated the averages over the next 2000 time steps. Keeping the final configuration, we changed the rules of a small number of sites, to bring $p(P2)$ down by 0.0025. We then continued the simulation, rejecting the first 250 time steps and averaging over the next 2000. This process was repeated down to $p(P2) = 0.60$ and back again to the initial concentration. Starting the run with $p(P2) = 0.60$ and going up and down again also produced hysteresis. Physically, this *first-order* transition happens because one cannot go continuously from an

Table 1. Scaling results for the QP3 to fixed-point transition. The fits were made for 0.0005 incremented p's.

L	p_c	γ
12	0.3600	0.75
16	0.3600	0.79
18	0.3590	0.75
20	0.3595	0.78
22	0.3600	0.80
24	0.3590	0.75

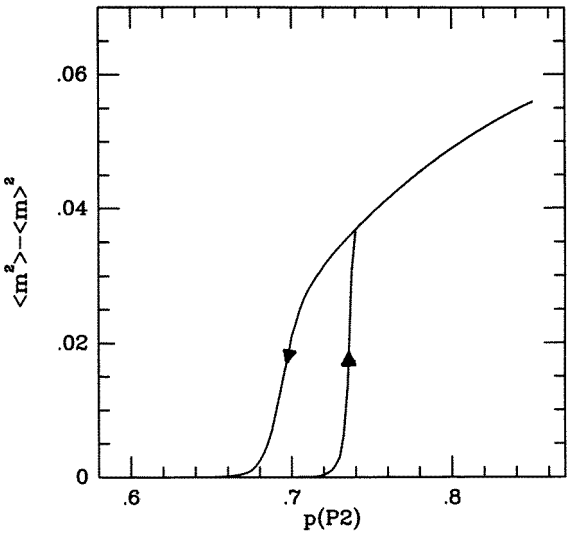

Figure 7. Hysteresis of the variance of the magnetization as a function of the concentration of rule P2 around the P2 to fixed-point transition. The starting point was at $p(\text{P2}) = 0.85$.

integer period to a fixed point. For this second transition, the critical probability is found to be at $p_c^{\text{P2}} = 0.70 \pm 0.03$. No hysteresis was found for the QP3 to fixed-point transition.

To study microscopic aspects of these CA, we follow the partial site–site autocorrelation functions:

$$C_p(t, t_0) = \frac{1}{N} \sum_{i \in p} \sigma_i(t + t_0)\sigma_i(t_0) \tag{7}$$

where p identifies the rule followed by the sites on which the average is taken and $\sigma = 2s-1$, rescaling the value of the spins to ± 1. Figure 8 shows that the qualitative behaviour of sites subjected to either rule is the same at a given concentration of rule P2. The only signature for the presence of different rules is found in the relative amplitude of the partial autocorrelations. In figures 8(b) and (c), the two branches correspond to even and odd times of the same correlation function. Similarly, in figure 8(a), we can observe the quasi-periodic oscillations in the autocorrelations as three intertwined series of symbols corresponding to times $(t - t_0) = 0, 3, 6, \ldots, 1, 4, 7 \ldots$ and $2, 5, 8, \ldots$. As is found for the total magnetization, autocorrelations in the cyclic phases do not display the presence of the minority rules; the only temporal oscillations are those related to the majority rule.

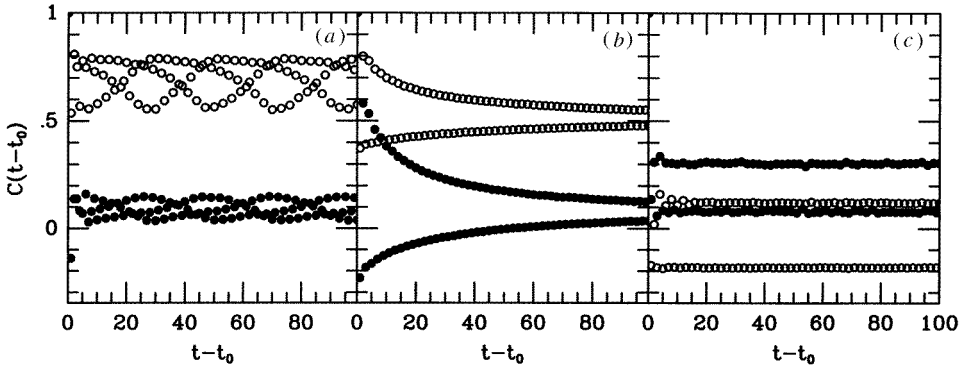

Figure 8. Time autocorrelation function (equation (9)) for sites following rule QP3 (full symbols) and sites following rule P2 (open symbols) at (*a*) $p(\mathrm{P2}) = 0.10$ and (*b*) $p(\mathrm{P2}) = 0.90$.

In a recent paper, Chaté *et al* [11] (CGT) used analogies with interface growth governed by the Kardar–Parisi–Zhang equation to study correlations in CA with the Hemmingsson rule. They made the prediction that the temporal decay of local fluctuations around the time-dependent global magnetization for quasi-periodic CA,

$$C'_p(t, t_0) = \frac{1}{N} \sum_{i \in p} \sigma_i(t + t_0)\sigma_i(t_0) - m_p^{\sigma}(t + t_0)m_p^{\sigma}(t_0) \tag{8}$$

with $m_p^{\sigma}(t) = 1/N_p \sum_{i \in p} \sigma_i(t)$, would follow

$$C'_p(t, t_0) \sim B(t, t_0)|t - t'|^{-(d-2)/2} \tag{9}$$

where $B(t, t_0)$ is an oscillating amplitude.

Since the CA studied here are in five dimensions, the envelope of decay should go like $-(d-2)/2 = -\frac{3}{2}$. One must note that this prediction applies only to quasi-periodic oscillations. Figure 9 shows that the relaxation in the QP3 region is *consistent* with CGT predictions in spite of a considerable amount of P2 rules. The relatively high level of background noise to which the autocorrelation converges rapidly, even with 164 million sites, makes it impossible to be more assertive. A similar situation is found in the decay of the autocorrelation for a CA with high concentration of rule P2 ($p(\mathrm{P2}) = 0.90$ in the results of figure 10). However, one can say with some confidence that the envelope of the decay is better approximated by an exponential than a power law. In agreement with CGT, the decay of the autocorrelations for the periodic phase do not follow (9).

For a pure-rule CA, it is not clear whether the autocorrelations defined by (8) go strictly to zero in the thermodynamical limit. Simulation with up to 500 million sites still shows a long-time limit converging to a very small but non-zero value (typically, around 10^{-3}–10^{-4}). One can be certain, however, that they converge to a non-zero value when impurities are introduced. Already at $p(\mathrm{P2}) = 0.90$, the higher and lower branches of the correlation decay to 0.073 and 0.003 for sites following rule P2 and 0.054 and 0.000 for those following rule QP3. Correlations also converge to a non-zero value in the QP3 region. We shall discuss this phenomenon in more detail in the next section.

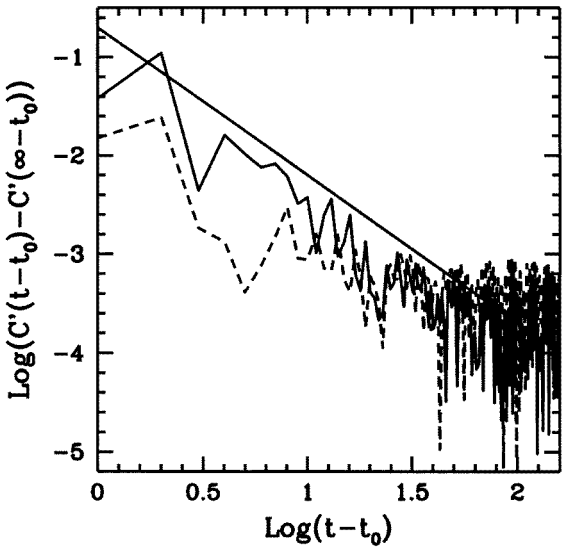

Figure 9. Log–log plot of the time autocorrelations (equation (10)) at $p(\text{P2}) = 0.10$. The long-time value has been subtracted independently for sites following rule QP3 (full curve) and P2 (broken curve), respectively. The full line indicates the slope proposed by Chaté *et al*. $t_0 = 1000$ and $L = 44$ (164 million sites).

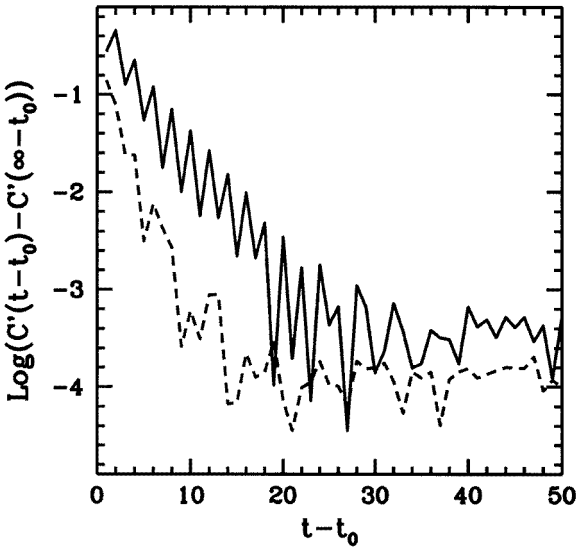

Figure 10. Log-normal plot of the time autocorrelations (equation (10)) at $p(\text{P2}) = 0.90$. The long-time value has been subtracted independently for sites following rule QP3 (full curve) and P2 (broken curve), respectively. $t_0 = 1000$ and $L = 44$ (164 million sites).

4. The glassy phase

We now examine in detail the central region of the phase diagram. Apart from some noise, the magnetization is constant in this region; cycles have disappeared at the macroscopic

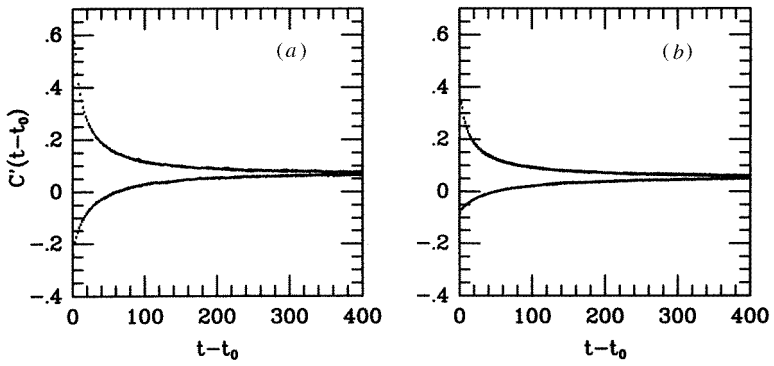

Figure 11. Time autocorrelation function (equation (10)) for rule (*a*) QP3 (*b*) P2 at $p(\mathrm{P2}) = 0.50$. Superimposed are the correlations with $t_0 = 100$ and $t_0 = 21\,000$.

level. In the Fourier spectrum of the magnetization at $p(\mathrm{P2}) = 0.50$, no single frequency dominates (figure 4). We find instead a large band of more or less constant amplitude.

Although in this region, the CA are macroscopically constant, they remain dynamically active at the microscopic level. The autocorrelation functions display both QP3 and P2 periodicity contrary to the global synchronization found in the two other phases.

For a 20^5 site lattice, partial autocorrelations (given by (8)), display in this region a very slow decay over more than a thousand time steps, in both periodic two and quasi-periodic three cycles. But the long-time value to which they decay is not zero and is rule-dependent (figure 11). As mentioned in the previous section, this non-vanishing long-time limit appears as soon as a second rule is introduced in the CA. This suggests that domains are introduced in which the temporal behaviour is strongly dominated by the local rules, increasing correlation between sites in these regions. On a five-dimensional lattice, it is difficult to imagine compact domains but one can think of strings or planes connected to each other. In the pure-rule CA, all sites are identical so that there is no defect preventing diffusion of information. As other rules are introduced, frustration appears which prevents full relaxation and can isolate regions. This can affect a relatively large proportion of sites, contributing up to about 10% of the amplitude of the time autocorrelation function. These values are much larger than what could be expected from the noise fluctuations. We can see these domains forming by looking at the distribution of the time-average autocorrelation function,

$$\langle C_i(t, t_0)\rangle_t = \frac{1}{t}\sum_{t'=t_0}^{t+t_0} S_i(t + t_0)S_i(t_0)\,. \tag{10}$$

For a pure-rule CA, this distribution is very peaked and, as expected, displays a Gaussian shape (figure 12(*a*)). As a second rule is introduced, the shape of this distribution becomes more complex with many Gaussian peaks appearing, mirroring the multiple local configurations available. In the glassy region, the distribution reaches the full width of the available values with an even smaller number of sites remaining frozen over more than 3000 time steps (figure 12(*b*)). This shape remains unchanged for different lattice sizes and initial configurations. It is therefore a signature of the glass phase.

The decay in the intermediate phase takes place on a much larger time-scale than in the periodic or quasi-periodic regions of the phase diagram. From figure 13(*a*), it is clear that the decay is much faster than a power law. In fact, the autocorrelations seem to follow a

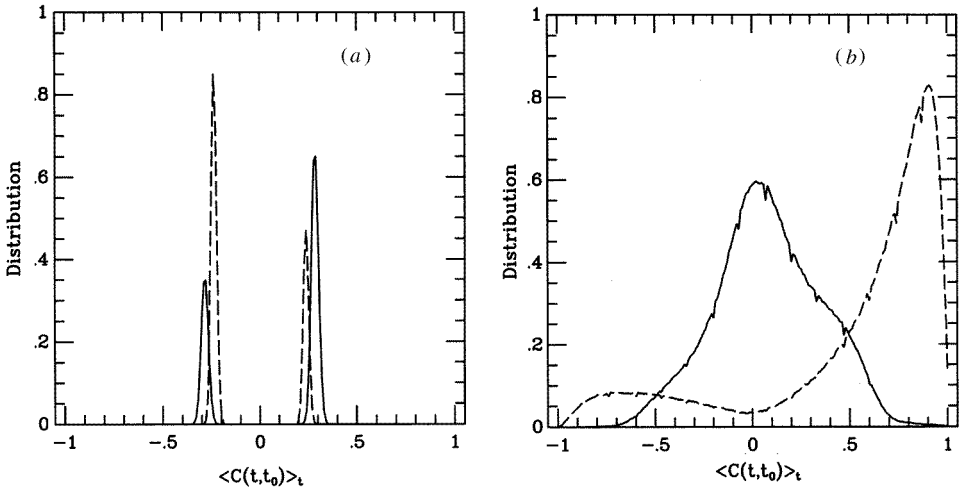

Figure 12. Distribution of the partial autocorrelation averaged over 3000 time steps. (*a*) Pure QP3 and P2 CA on 15^5 site lattices; (*b*) $p(\mathrm{P2}) = 0.50$ on a 20^5 site lattice. Full curve, sites following rule QP3; broken curve, sites following rule P2.

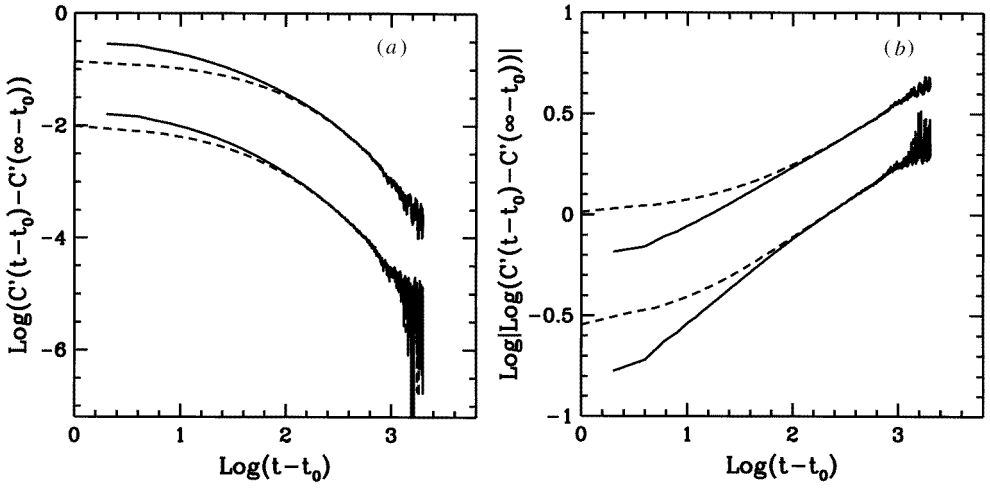

Figure 13. (*a*) Log–log plot and (*b*) log–double-log plot of the time autocorrelation with the long-time value subtracted for sites following rule QP3 (two higher curves) and (*b*) P2 (two lower curves). The full curves are for the higher branches, the broken curves for the lower branches as shown in the previous figure. The curves have been translated vertically for better display. $t_0 = 1000$ and $L = 44$.

stretched exponential:

$$C_{\mathrm{p}}(t, t_0) - C_{\mathrm{p}}(t, \infty) \sim \exp(-t^{\beta}) \tag{11}$$

with $\beta < 1$. This relaxation is reminiscent of what is found in glasses and spin glasses, but happens here at zero external noise. Figure 13(*b*) shows the log–double-log plot for the upper and lower branches of correlations at $p(\mathrm{P2}) = 0.50$ for sites following QP3 and P2 rules, respectively. In both cases, the long-time values of these autocorrelations have been subtracted. The exponent β depends both on the rule followed and the concentration

p(P2). β is therefore not a universal quantity. Moreover, the different branches of the autocorrelation do not converge on the stretched exponential with the same time. The upper ones fall almost immediately onto a straight line while the process can take up to almost a hundred time steps, at $p(\text{P2}) = 0.50$, for the lower branches. In both cases this is very much faster than what is typically found in normal glasses where the stretched exponential relaxation (or the β relaxation) sets in only in the long-time limit. Contrary to normal glasses where we find two regimes of relaxation, we find only one here which is completely described by the exponent β.

As can be seen from figure 11, the relaxation is completely independent of the initial time t_0. There is no detectable difference between the relaxation with $t_0 = 1000$ and 21 000 and therefore no ageing. This is not what is found in other frustrated systems like glasses or spin glasses where ageing is important. It could be due to the fact that the system studied is *basically* dynamical, i.e. that under the glass dynamics lies another one controlled by the updating rules. While conventional glasses reach a stable state in the infinite time limit, this may not be possible in our CA since it lacks any cost function to minimize, ruling out ageing.

The physical origin of the stretched exponential is not completely clear in this model. The non-zero value to which the correlations decay signals the presence of quasi-frozen domains. It is therefore not unreasonable to suppose that these domains possess different relaxation times. Superposition of all these domains could then lead to a global stretched exponential behaviour as has been proposed for conventional glasses. The presence of a first-order transition between the central and P2 phases could explain the presence of domains which, although not leading to a periodic macroscopic behaviour, could slow down considerably the dynamical relaxation in trying to get the whole system fully synchronized.

Is this phase glassy? The stretched exponential would surely lead us to conclude that this is the case. In systems with detailed balance, quenched disorder of competing rules can lead to a glassy dynamics but we are dealing with a non-equilibrium system. Moreover, not all signatures of a glass are present here. In particular, there is no ageing effect on the autocorrelation functions. But the CA studied are fundamentally dynamical objects where the glassy dynamics is superimposed onto an intrinsic periodic or quasi-periodic one. The frustration is between two temporal behaviours, not two incompatible local stable states. It is in this respect that this is a glassy phase, with sites unable to fall on the synchronized period favoured by each rule.

5. Effects of external noise

In their review paper [8], Chaté and Manneville discussed the stability of the cycles under the introduction of bounded noise that changes a site from one to zero with a certain probability. This type of noise leads to an absorbing and irreversible state. In this work we consider noise that pushes the system to a paramagnetic state where sites with value 0 and 1 can be found with equal probability, analogous to the effect of temperature in equilibrium spin models. After each deterministic update, the value of a site is changed (from one to zero or vice versa) with a probability η, leading to unbounded noise. Because there is no cost function, a Boltzmann distribution is not applicable and the probability of changing a site is independent of its local configuration.

At high noise levels, we expect that correlations between the sites will be completely lost and therefore that the simple mean-field solution of Chaté and Manneville, supplemented by a deterministic noise term, should describe the model. Since the process is done in parallel on all the sites, we first calculate deterministically the magnetization m^* with (3) and then

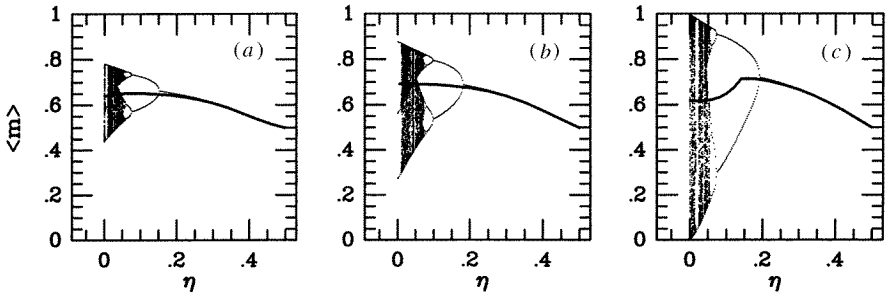

Figure 14. Magnetization as a function of external noise η for (*a*) $p(\text{P2}) = 0.00$, (*b*) $p(\text{P2}) = 0.50$ and (*c*) $p(\text{P2}) = 1.00$. The full curve is from simulation and dots are from the mean-field solution.

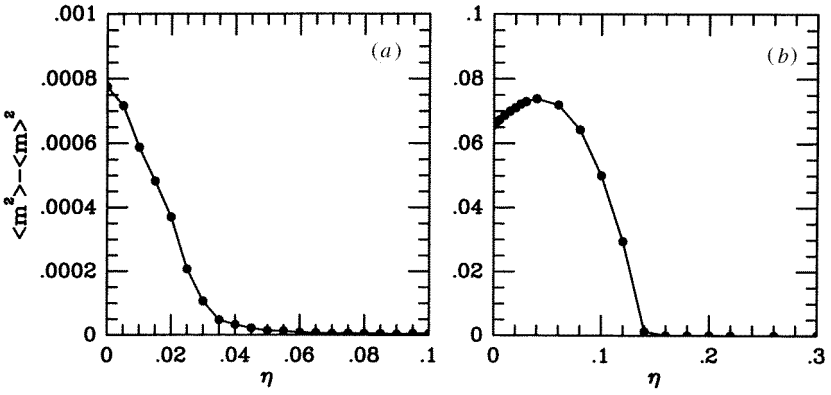

Figure 15. Δm as a function of external noise for pure (*a*) QP3 and (*b*) P2 CA.

add the effect of the noise:

$$m(t+1) = m^*(t+1) - 2\eta(m^*(t+1) - 0.50)\,. \tag{12}$$

In the absence of noise, this equation leads to chaotic temporal behaviour for pure P2 and QP3 CA. With the introduction of noise, the mean-field solution goes through the usual doubling route from chaos and reaches a single-valued fixed point for noise larger than about 20%. It is interesting to note that the mean-field solution and the direct simulation are almost equal when the former becomes single valued.

In figure 14, we follow the effects of noise on the magnetization for pure QP3 $p(\text{P2}) = 0.50$ and pure P2, respectively. The states reached by adding noise are fully reversible so that it is possible to go back and forth from any phase to any other. This reversibility indicates that the periodic and quasi-periodic cycles found at low external noise correspond to a unique stable low-temperature limit. Figure 15 displays the variation of the size of the cycle as a function of external noise for pure QP3 and P2 CA. For pure QP3, the critical external noise, i.e. the point where Δm goes almost to zero, is located at $\eta \approx 0.05$. For the pure P2 CA, we find a phase transition at $\eta \approx 0.15$.

For the central glassy phase, the autocorrelation relaxation changes from a stretched exponential to power-law decay at $\eta \approx 0.20$ (see figure 16). The correlation time is very short and tends to 1 at $\eta \approx 0.30$. At high noise levels we recover the behaviour found in the other phases, and therefore a transition exists from the glassy phase to the disorder phase.

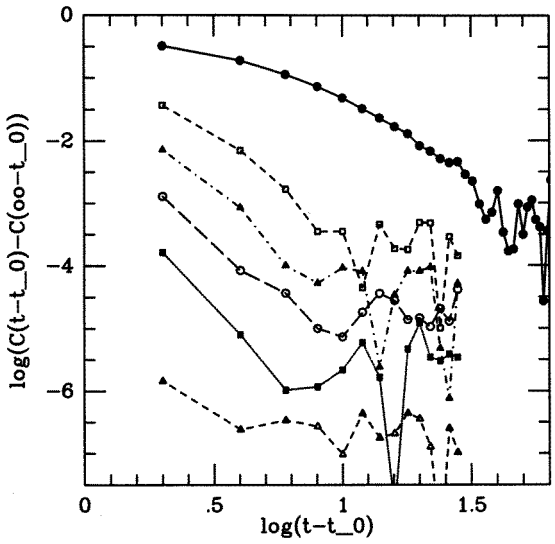

Figure 16. Log–log graph of the higher branch of the time autocorrelation function with the long-time value subtracted for sites following rule QP3 with $t_0 = 1000$. Concentration of rule p(P2) $= 0.50$, lattice size 20^5 sites. Full circle, $\eta = 0.04$; open squares, $\eta = 0.16$; full triangles, $\eta = 0.20$; open circles, $\eta = 0.24$, full squares, $\eta = 0.28$ and open triangles, $\eta = 0.32$. Points have been shifted for better display. The curves are a guide for the eyes.

6. Other rules

All the results presented in the previous sections were for a mixture of rules $\mathcal{R}^5_{5-8}$ and $\mathcal{R}^5_{1-9}$. We also examined other pairs of Chaté–Manneville-type rules: $\mathcal{R}^5_{1-2}$ or $\mathcal{R}^5_{1-7}$ (both period two) combined with $\mathcal{R}^5_{4-7}$, $\mathcal{R}^5_{4-8}$, $\mathcal{R}^5_{4-9}$, $\mathcal{R}^5_{5-8}$, $\mathcal{R}^5_{5-9}$ or $\mathcal{R}^5_{5-10}$ (displaying QP3 behaviour). At zero external noise, they presented a phase diagram similar to what is obtained in the mixture $\mathcal{R}^5_{5-8}$ and $\mathcal{R}^5_{1-9}$: cycles are stable under finite amounts of impurity and fall onto fixed points when the concentration of impurities becomes too large. In general, QP3 cycles appear less stable under frustration than the periodic two-cycles.

None of these pairs of rules presents a richer phase diagram than what is discussed above. This statement does not constitute a proof that frustration could not cause different behaviour for carefully chosen pairs but it indicates that the phase diagram presented in the previous section could be the norm in these dynamical frustrated models.

7. Conclusion

We have studied the phase diagram of Chaté–Manneville cellular automata in which frustration is introduced by quenching two different dynamical rules on the lattice sites. As the concentration of one rule varies, the CA go through two phase transitions, one first and the other second order. With low amounts of impurities, the CA become less chaotic and intrinsic noise levels are decreased. The time behaviour of the minority rule is not detected either macroscopically or microscopically if its concentration is low. In the region between the two phase transitions, the CA is macroscopically constant while presenting a signature of a glass phase in the autocorrelation functions. This is a special glass phase since its slow dynamics is superimposed on the much faster dynamics of the rules. No signs of ageing

have been detected.

These CA remain stable with either internal frustration or external stochastic noise. As the external noise level increases, the macroscopic order parameter reaches a fixed value which can be described by a mean-field equation. This process is perfectly reversible indicating that the periodic or quasi-periodic cycles are the thermodynamical states of these rules in the low-noise phase.

Most interesting, perhaps, is the fact that these results are not particular to a single pair of rules but appear generally in these CA. It should therefore be possible to extend the application of these results to other more realistic systems.

Acknowledgments

I would like to thank H Chaté, M Henkel and D Sherrington for helpful discussions and G Barkema for implementing the multispin code. I would also like to thank both G Barkema and D Sherrington for a critical reading of this manuscript. Finally, I am grateful to the Natural Sciences and Engineering Research Council of Canada for a postdoctoral fellowship.

References

[1] Wolfram S (ed) 1986 *Theory and Applications of Cellular Automata* (Singapore: World Scientific)
Boccara N (ed) 1993 *Cellular Automata and Cooperative Systems (NATO ASI Series C 396)* (Dordrecht: Kluwer)
[2] Frisch U, Hasslacher B and Pomeau Y 1986 *Phys. Rev. Lett.* **56** 1505
[3] Toulouse G 1977 *Commun. Phys.* **2** 115
[4] Yeomans J 1988 *Solid State Phys.* **41**
[5] See, for example, Fischer K H and Hertz J A 1991 *Spin Glasses* (Cambridge: Cambridge University Press)
[6] Mousseau N 1994 *Europhys. Lett.* **28** 551; 1995 *Europhys. Lett.* **29** 269 (erratum)
[7] Chaté H and Manneville P 1991 *Europhys. Lett.* **14** 409
[8] Chaté H and Manneville P 1992 *Prog. Theor. Phys.* **87** 1
[9] Hemmingsson J 1992 *Physica* **183A** 255
[10] Grinstein G, Mukamel D, Seidin R and Bennett Ch H 1993 *Phys. Rev. Lett.* **70** 3607
[11] Chaté H, Grinstein G and Tang L-H 1995 *Phys. Rev. Lett.*
[12] Gallas J A C, Grassberger P, Herrmann H J and Ueberholz P 1992 *Physica* **180A** 19
[13] Hemmingsson J and Peng Gongwen 1994 *J. Phys. A: Math. Gen.* **27** 2235
[14] Hakim V and Rappel W-J 1994 *Europhys. Lett.* **27** 637